Hindawi
Advances in Civil Engineering
Volume 2022, Article ID 2722831, 9 pages
https://doi.org/10.1155/2022/2722831

Research Article

Stress-Strain Relationships and Failure Load Analysis of Cement-Stabilized Rammed Earth under Concentric and Eccentric Loading Using Finite Element Modelling

B. M. Sreedhara,[1] **M. Rahul Raj**,[1] **Geetha Kuntoji**,[2] **Sujay Raghavendra Naganna**,[1] **and Zaher Mundher Yaseen**[3,4]

[1]*Department of Civil Engineering, Siddaganga Institute of Technology, B. H. Road, Tumakuru 572 103, Karnataka, India*
[2]*Department of Civil Engineering, B. M. S. College of Engineering, Bengaluru 560 019, Karnataka, India*
[3]*Department of Earth Sciences and Environment, Faculty of Science and Technology, Universiti Kebangsaan Malaysia, Bangi 43600, Selangor, Malaysia*
[4]*New Era and Development in Civil Engineering Research Group, Scientific Research Center, Al-Ayen University, Nasiriyah, Thi-Qar 64001, Iraq*

Correspondence should be addressed to Zaher Mundher Yaseen; yaseen@alayen.edu.iq

Received 25 May 2022; Revised 24 June 2022; Accepted 7 July 2022; Published 2 August 2022

Academic Editor: Khaled Ghaedi

Among many alternative building materials, soil in the form of rammed Earth is the most ancient construction material and technology. Large-scale application of the rammed Earth technology in the construction industry requires the assessment of its strength and failure behaviour. Therefore, this study focused on performing a nonlinear stability analysis of cement-stabilized rammed Earth (CSRE) specimens having a height-to-thickness (H/T) ratios—3 and 4 and loaded under varying degrees of eccentricities 0, 1/3, 1/6, and 1/12. The maximum compressive strength and the stress-strain behaviour of the CSRE specimens were determined through finite element (FE) modeling. The experimental results of the cement-stabilized rammed Earth (CSRE) have been obtained from literature for validation by FE simulation. As the H/T ratio was increased from 3 to 4, the load-bearing capacity of the CSRE specimens increased by 2.91% under concentric loading condition; however, when the eccentricity of load application was swapped from 0 to 1/12, 1/6, and 1/3, the load-bearing capacity decreased incrementally. The results of the FE analysis of the specimens showed that the compressive strength and elastic properties of the CSRE specimens did not differ significantly. The stress-strain relationships were nonlinear and elastic properties were affected by soil textural composition and density.

1. Introduction

Various materials are used in the construction industry from simple to complex constructions [1]. Some are naturally available materials such as wood/timber and soil, and some are man-made like cement, steel, and bricks. The production of the conventional construction materials such as cement and steel involves the consumption of a huge amount of raw materials and energy along with the release of millions of tons of waste/by-products, noise, dust, and toxic gaseous emissions such as sulphur dioxides, and oxides of nitrogen and carbon. The CO_2, a greenhouse gas, one of the major culprits in environmental deterioration, is produced in the highest amount during the manufacturing process of cement. Along with this, the transportation of these building materials to the site will also witness the emission of CO_2 from the automobiles. Hence, there is an urgent requirement to innovate or bring changes in the building materials that meets the sustainability and structural stability criteria for the greater good of the environment and the society [2]. Among many alternative sustainable building materials available, a historical rammed Earth construction

technology that uses natural subgrade soil as a raw material has recently started gaining popularity [3]. Rammed Earth has been perceived as a fast, simple construction method for the construction of defensive walls in an economical way; build dwellings; and a sustainable way of construction that uses only whatever is accessible on site [4]. This technology basically involves the placing of soil between the formwork boards in layers and compacting it to the required density, to build a homogeneous wall mass. Modern era engineers typically consider rammed Earth technology as a response to the question of making residences for people with restricted financial capital [5].

Usually, the soil to be used in rammed Earth construction should have more clay content since it provides the cohesion between the material particles, which is required for ensuring the stability of the constructed structure. The topsoil is usually not used in the rammed Earth construction process, as it contains biodegradable organic material and absorbs water easily, and also at times, it can be compressed to a large extent, which is not preferred for rammed Earth construction [6]. There are two categories of mixtures in rammed Earth material such as unstabilized and stabilized. The stabilized rammed Earth consists of a mixture of soil, aggregates, and additives, which can be inorganic or organic (cement or lime) that act as a stabilizer to improve the overall strength and performance of the rammed Earth [7], whereas unstabilized rammed Earth does not use any additives and consists of only Earth; that is, the only binder is clay of the soil. The minimum permissible compressive strength values for unstabilized rammed Earth vary from 0.25 MPa to 0.6 MPa, while values for stabilized rammed Earth range between 1 MPa and 15 MPa, although this obviously depends on the amount of stabilizer added [8]. There is a substantial increase of using the rammed Earth construction method in developed countries such as United Kingdom, Australia, the United States of America, and New Zealand owing to global sustainable construction agenda. These countries have developed guidelines, codes, standards, or reference documents for the rammed Earth construction [9–13]. Unfortunately, in India, due to the lack of material testing and case studies on rammed Earth, there are no separate guidelines, standards, or national reference codes being formulated for earthen buildings, and therefore, masonry codes and guidelines are still being followed.

Extensive research is available on rammed Earth technology by various researchers considering both stabilized and unstabilized mixes. The geotechnical properties of the soil play a very important role in rammed Earth construction, and these properties will suggest the suitability of soil. Burroughs [14] considered linear shrinkage and plasticity index as the key indicators for determining the suitability of soil. The range of permissible percentage of shrinkage varies from 0.05% to 3%. Despite decades of research, some countries still design the structural rammed Earth structural elements using suitable Earth, considering the masonry design rules [15]. The structural components like wallets and prisms are usually used to study the compressive strength of rammed Earth of different height-to-thickness ratios. Data from several studies suggest that the strength reduces by about 30 percent on increasing the height-to-thickness ratio from 5 to 20 [16, 17]. Rammed Earth supports for the construction of ideal sustainable housing units satisfying both eco-friendly and structural stability parameters [18, 19]. Based on the knowledge of weathering processes that dominate in any given area, rammed Earth construction can be undertaken using locally available soil designed to obtain suitable strength and durability characteristics using stabilizers [3, 20–22]. Bui et al. [23] in practice found that the tensile and shear strengths of rammed Earth to be around 10 percent of the strength under compression. A comprehensive review by Ávila et al. [24] provides extensive information on the characterization of unstabilized rammed Earth constructions, considering all mechanical, thermal, and acoustic properties. Finite element modeling has been recognized by a number of researchers as a viable method for investigating the mechanical behaviour of rammed Earth units. Chazallon and Chazallon [25] present elastoplastic modeling of a rammed Earth wall based on finite element simulation to study the hydro-mechanical behaviour of rammed Earth construction under static loading. Similarly, for out-of-plane loading conditions, Shrestha et al. [26] simulated finite element models to predict the response of the rammed Earth building components. Also recently, Strazzeri et al. [27] incorporated micromechanics approach to build a multiscaling model that predicts the macroscopic linear elastic behaviour of cement-stabilized rammed Earth (CSRE) taking into account of material heterogeneities. Over time, an extensive literature on laboratory tests conducted by changing soil properties to study the strength and stability of rammed Earth elements (such as prism, wallets, and full-scale wall for different slenderness ratios under both concentric and eccentric loading conditions) reveals a number of gaps and shortcomings. To check the suitability of soil for rammed Earth construction, different soil properties, and strength and stability of different rammed Earth elements such as prism, wallets, and full-scale wall can be studied using finite element modeling. There is very limited research on the analytical studies of rammed Earth using a finite element analysis to understand its nonlinear behaviour through finite element modeling [25, 28]. Hence, in this study, the objective was to analytically determine the compressive strength and stress-strain behaviour of cement-stabilized rammed Earth (CSRE) elements with different H/T ratios (3 and 4) under different load eccentricities (0, 1/3, 1/6, and 1/12) as per Indian Masonry code IS 1905–1987 [29].

2. Methodology

2.1. Experimental Data. The data of cement-stabilized soil required for the finite element analysis of rammed Earth specimens were collected from literature titled "Strength and durability of rammed Earth for walling" [22]. The suitability of soil properties and their range for rammed Earth construction were taken from the literature titled "Behaviour of cement-stabilized rammed Earth walls under concentric and eccentric gravity loading" [17].

The locally available soil was used in the experimental works of literature [22], and their properties are tabulated in Table 1. The soil property data conformed to be within the

Table 1: Properties of soil used for modeling.

Textural composition	
Sand (0.075–4.75) mm	61%
Silt (0.002–0.075) mm	17%
Clay (<0.002) mm	22%
Atterberg's limits	
Liquid limit	29
Plastic limit	22
Shrinkage limit	20
Plasticity index	7
Shrinkage index	9
Maximum dry density (kg/m^3)	2020

Adopted from Suresh and Anand [22].

range of basic soil properties necessary for rammed Earth structures as per literature [17]. Finite element modeling was carried out, and the obtained results were compared and validated with the previous research [22] for concentric loading conditions. The study was further extended by considering cement-stabilized rammed Earth specimens for different H/T ratios (3 and 4) and under different eccentricities (0, 1/3, 1/6, and 1/12) to determine the compressive strength and stress-strain behaviour.

2.2. Finite Element Modeling. A method that was used primarily to solve the partial differential equations numerically is termed as the finite element method or finite element analysis [30]. In simple terms, a physical phenomenon is discretized into smaller or simpler elements, which are then solved to obtain the overall solution by combining the solutions of smaller elements. These discretized elements are referred to as finite elements. The finite elements are connected to each other by nodes. This whole system of finite elements and the nodes is called as a mesh. The mesh is simply a system of mathematical equations, whose unknowns are the values of dependent variables in nodes. The equations are solved using the nodal values of dependent variables. The value of the whole element is found using shape functions. Thus, a piecewise approximation of spatial variation in dependent variables is obtained [31]. The Newton–Raphson method was used to solve the system of nonlinear equations and for the refinement of the finite element mesh. In this study, a macromodeling approach was considered in the ANSYS software platform for implementing finite element analysis.

2.3. Modeling Considerations and Calibration. The prism specimen of dimension 150 mm × 300 mm × 450 mm of (H/T = 3) was modeled, in three layers with a lift of 150 mm similar to the construction technique where the soil is rammed or compacted in layers of 150 mm. The mild steel plate is considered on top of the specimen for the application of load in order to avoid direct application of load on the specimen, which may cause local failure of the specimen. The thickness of the mild steel plate considered was 20 mm. The geometry modeled should be assigned with the material properties in order to carry out the analysis. The material properties considered for the study are as follows:

(1) Soil + 7% cement

(2) Structural steel (plate)

For the materials defined, various properties have to be assigned as inputs such as density, young's modulus, Poisson's ratio, and specimen dimensions in order to perform the nonlinear analysis in ANSYS workbench [32]. The input of stress and strain values of the material is mandatory for performing nonlinear analysis. The required stress and strain values of the material were taken from the experimental investigation [22]. The contact region between the layers of the elements should be connected by some sort of connections like rigid or frictional surface. The connections between the layers are usually automatically generated by the ANSYS workbench, but it is always preferred to create the connections again according to our requirements. In this study, the rammed Earth prism specimen was modeled as a set of stacked layers (of 150 mm) of finite elements to simulate the interfaces between compaction layers. The interface between the layers has to be connected to one another. This can be done using the connection options in ANSYS. In this case, frictional contact was used between the topmost soil layer and mild steel plate; and bonded contact was used between the stacked soil layers. A global coordinate system was considered in this study.

ANSYS being an FEM analysis tool, the specimen or model will be divided into finite elements, and each element will be analysed from the given inputs. Here, the model is divided into finite elements by meshing. Any mesh size can be assigned, but considering the system features and the capacity to simulate, the corresponding mesh size should be given as input, because as we decrease the mesh size, the number of elements increases and as the number of elements increases, the software has to analyse each element; hence, the simulation/analysis time would increase. The mesh size given as input in our case was 10 mm. The basic idea behind finite element analysis is that the analysis of each step is divided into the specified number of substeps till the result converges to the inbuilt reference of ANSYS workbench. Therefore, in this study, the maximum number of substeps assigned was 15. The support conditions for the FE model were assigned as "FIXED" at the base of the prism specimen. A concentric uniformly distributed compressive load was applied on the specimen through a mild steel plate. The uniformly distributed compressive load was incrementally increased at the rate of 10 kN till failure in the finite element analysis. However, during analysis after the application of certain incremental load, the loading rate changes to 1 kN in order to obtain the exact failure load of the specimen due to compression. Prior to failure, the CSRE prism elements are considered to be linearly elastic and isotropic. Final failure of CSRE prism elements is indicated by the lack of symmetry in the displacements or by the convergence of the displacements. The results obtained from the modeling for concentric loading were validated with the experimental results of the literature [22].

Furthermore, this study was extended to analyse the behaviour of prism specimens (150 mm × 300 mm × 600 mm) with H/T = 4 at different ratios of eccentricity (E/T) as given below:

(i) Specimen—1 (150 mm × 300 mm *x* 450 mm): H/T = 3 and E/T = 0 (concentric load)

(ii) Specimen—2: H/T = 3 and Load at E/T = 1/3 (50 mm from the axis along the thickness)

(iii) Specimen—3: H/T = 3 and load at E/T = 1/6 (25 mm from the axis along the thickness)

(iv) Specimen—4: H/T = 3 and load at E/T = 1/12 (12.5 mm from the axis along the thickness)

(v) Specimen—5 (150 mm × 300 mm × 600 mm): H/T = 4 and E/T = 0 (concentric load)

(vi) Specimen—6: H/T = 4 and Load at E/T = 1/3 (50 mm from the axis along the thickness)

(vii) Specimen—7: H/T = 4 and load at E/T = 1/6 (25 mm from the axis along the thickness)

(viii) Specimen—8: H/T = 4 and load at E/T = 1/12 (12.5 mm from the axis along the thickness)

3. Simulation Results and Discussion

3.1. Analysis of CSRE Prism Specimen under Concentric Loading. The CSRE prism specimen with H/T = 3 was considered to study the deformation, failure load, and stress-strain behaviour under concentric loading, and the model results were validated with the experimental results. Figure 1 shows the FE model of CSRE specimens. The incremental load of 10 kN was applied to study the deformation of prism specimen, and the maximum load taken by the specimen was found to be 103 kN with 5.38-mm deformation. The CSRE prism loaded at the centroid of the cross section demonstrated increased load-bearing capacity (failure load) as the H/T ratio was increased from 3 to 4, owing to homogeneous longitudinal stress distribution along the height of the prism and the absence of local buckling (which occurs only when the height-to-thickness ratio is greater than 10). Table 2 shows the comparison of the FE model results and the experimental results. A root mean square error of 1.95 mm was obtained between the model and experimental results. Stress and strain values observed at the centre of the specimen were noted for different loading intensities until failure and a stress v/s strain curve was plotted for the same as shown in Figure 2. CSRE specimen failure results from a unique and critical combination of biaxial stresses. Under concentric loading conditions, the load-carrying capacity of CSRE prisms was relatively higher, and the tendency for out-of-plane deformation was lower. It could be observed from the stress-strain curve that the FEM model is following the same trend and has good correlation with the experimental results. The FE model results validated against the experimental results encouraged for further study of CSRE specimens with varying H/T ratios under different eccentric loading conditions.

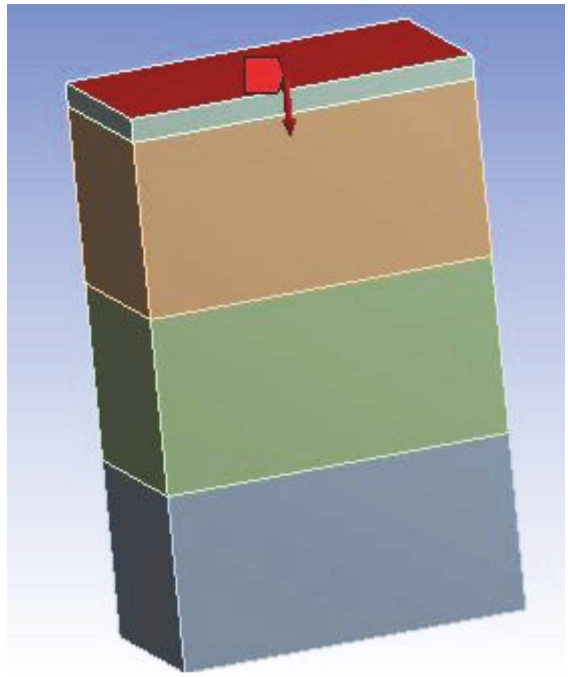

Figure 1: FEM model of CSRE prism (H/T = 3) under concentric loading.

3.2. Analysis of CSRE Prism Specimen under Eccentric Loading with H/T = 3. The CSRE prism (specimen size—150 × 300 × 450 mm) with H/T = 3 was considered for the FE modeling and analysed under different eccentric loading conditions to obtain the maximum compressive strength as well as stress and strain values at the centre of the specimen. The FE models of the specimen with H/T = 3 under different load eccentricities are shown in Figure 3. Figure 4 shows the deformation curve of the CSRE specimen with H/T = 3 under 4 different eccentricities, that is, 0, 1/3, 1/6, and 1/12. It was found that the maximum compressive load of the specimen decreases as the eccentricity of load application increases. On average, the compressive strength decreases by 32% as the eccentricity increases from 0 to 1/6, while it decreases to 42.8% when eccentricity is changed from 1/6 to 1/3. The deformation contours presented in Figure 5 indicate that the deformation was maximum at the top and minimum at the bottom. A faster loss of stability could be seen when the load eccentricity increases leading to a reduced compressive strength of prism specimens.

The maximum stress and strain values of each specimen at the centre are tabulated in Table 3. The stress values of the specimen remain the same for eccentricities 0 and 1/12, and on average, it decreases by 31.08% as the eccentricity is increased from 1/6 to 1/3. The strain of the specimen decreases by 43.47% on average as eccentricity is increased from 1/12 to 1/3, whereas the strain value for eccentricity 0 is 3 times lesser than that of eccentricity—1/12. The stress values add up in the specimen under eccentric loading due to the moment created by the load, which can be found manually using the bending equation. The strain within the specimen increases with an increase in the eccentricity as

Table 2: Load-deformation values of CSRE prism (H/T = 3; E/T = 0).

Load (kN)	Deformation (mm)		% error	Root mean square error (mm)
	Finite element model (M_i)	Experimental (E_i)	$= (M_i - E_i)/E_i \times 100$	$= \sqrt{\sum_{i=1}^{N} (M_i - E_i)^2/N}$
0	0	0	0	
10	0.506	0.6	15.67	
20	1.04	1	3.85	
30	1.56	1.47	5.77	
40	2.09	1.85	11.49	
50	2.6	2.35	9.62	1.95
60	3.15	2.65	15.88	
70	3.7	2.9	21.63	
80	4.29	3.3	23.08	
90	4.91	3.5	28.72	
100	5.22	4	23.38	
103	5.38	4.35	19.15	
104	Failure load		Mean = 14.85	

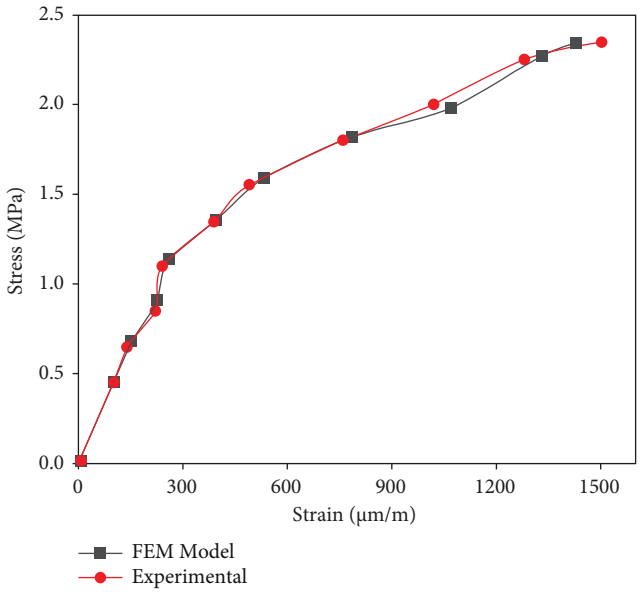

Figure 2: Stress-strain curve at the centre of CSRE prism with H/T = 3 under concentric loading.

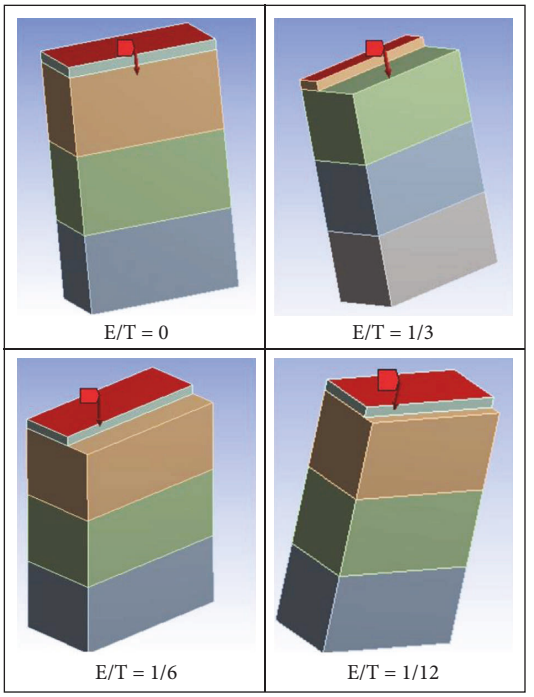

Figure 3: CSRE specimens with H/T = 3 models at different eccentricities.

shown in Figure 4. This demonstrates how the eccentric load affects the rigidity of the CSRE prism, leading the specimen to lose stability more quickly. Furthermore, when the eccentricity of the load increases, the load-bearing capacity of the prism specimen decreases monotonically.

3.3. Analysis of CSRE Prism Specimen under Eccentric Loading with H/T = 4. The CSRE prism (specimen size—150 × 300 × 600 mm) of H/T = 4 with different eccentricities were modeled and analysed in a similar fashion as that of the CSRE specimen of H/T = 3, to obtain the maximum compressive strength and stress v/s strain behaviour at the centre. Different material properties can be defined in the FE model to simulate the changes in the behaviour of the entire unit considered. In the model with H/T = 4, another layer of cement-stabilized soil was placed on the previous layer with a lift of 150 mm to obtain an overall specimen height of 600 mm. The connection between the layers of soil was bonded in nature. The models of the specimen with H/T = 4 with different eccentricities are shown in Figure 6. Figure 7 shows the deformation curves of the specimens with H/T = 4 under four different eccentricities, that is, 0, 1/3, 1/6, and 1/12. The maximum compressive strength of the specimen on an average decreases by 33.96% when the eccentricity is increased from 0 to 1/6, while it decreases by 42.8% when the eccentricity is further increased from 1/6 to 1/3. The CSRE prism loaded at the centroid of the cross section demonstrated increased load-bearing capacity (failure load) as the H/T ratio was increased from 3 to 4, owing to homogeneous longitudinal stress distribution along the height of the prism and the absence of

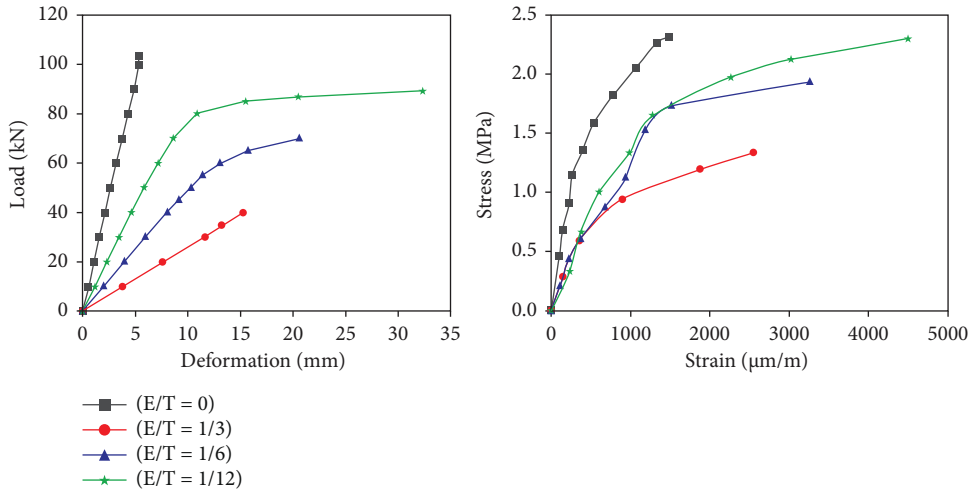

Figure 4: Load-deformation curve and stress-strain curves at the centre for CSRE specimens with H/T = 3.

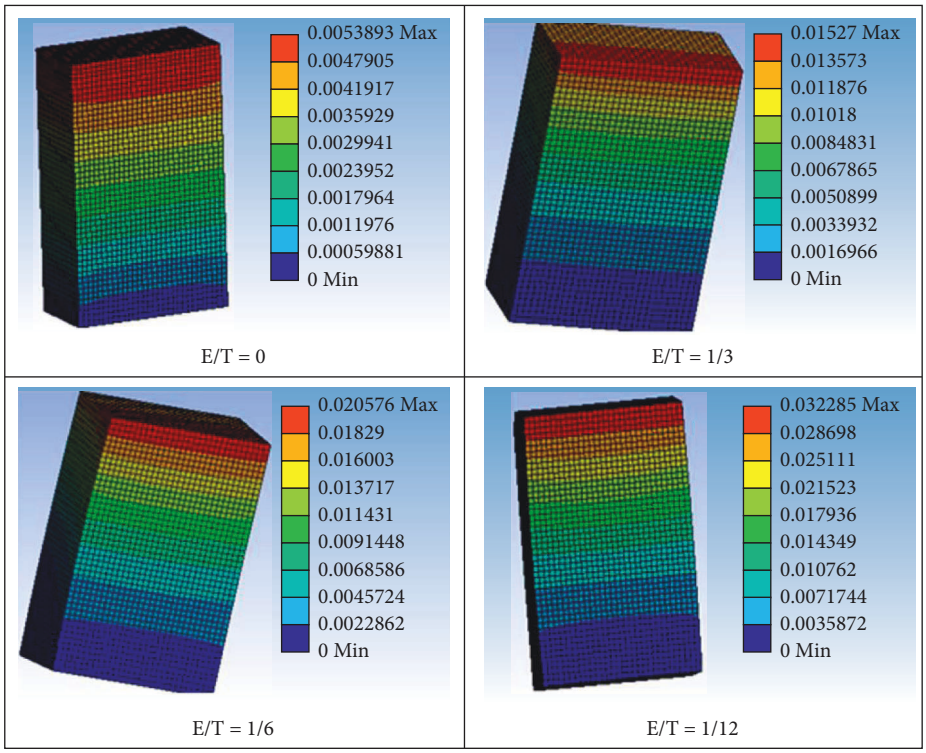

Figure 5: Deformation contours of specimens with H/T = 3.

Table 3: Result summary of the finite element model of CSRE specimens.

Eccentricity ratio	E/T = 0		E/T = 1/3		E/T = 1/6		E/T = 1/12	
CSRE prism specimens	H/T = 3	H/T = 4	H/T = 3	H/T = 4	H/T = 3	H/T = 4	H/T = 3	H/T = 4
Failure load (kN)	103	106	40	40	70	70	89	88
Maximum deformation (mm)	5.38	7.77	15.27	25.62	20.57	37.90	32.30	47.90
Maximum stress (MPa)	2.31	2.33	1.33	1.29	1.93	1.72	2.30	2.29
Maximum strain (μm/m)	1428	1460	2538	2705	3258	3210	4490	4405

local buckling (which occurs only when the height-to-thickness ratio is greater than 10). The deformation contours shown in Figure 8 indicate that the deformation was maximum at the top and minimum at the bottom. The stress v/s strain curves drawn for the CSRE specimen with H/T = 4 under different eccentric loading conditions are presented in

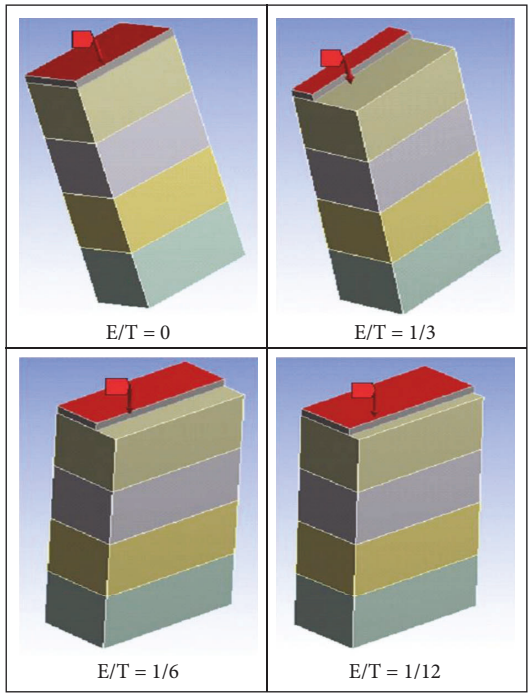

Figure 6: CSRE specimens with H/T = 4 models at different eccentricities.

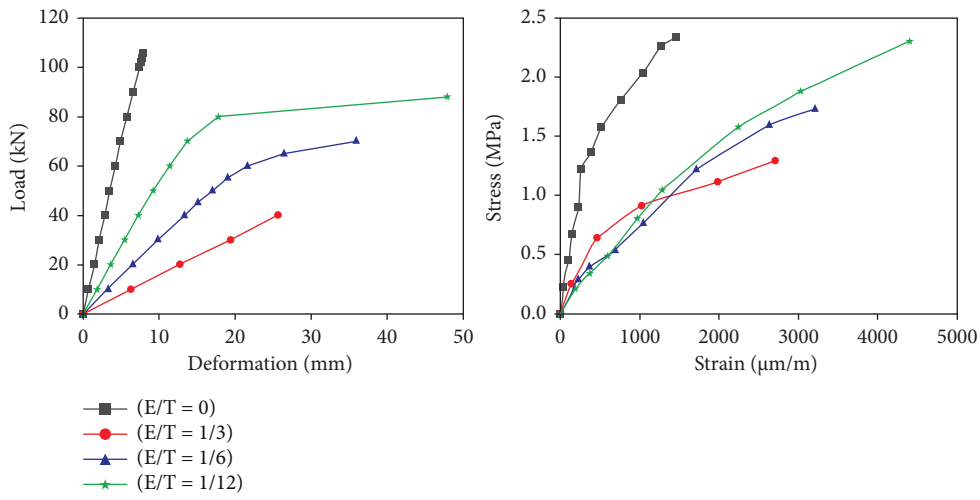

Figure 7: Load-deformation curve and stress-strain curves at the centre for CSRE specimens with H/T = 4.

Figure 7. The stress value of the specimen almost remains the same for the eccentricities 0 and 1/12, whereas on average, it decreases by about 25% when the eccentricity is increased from 1/6 to 1/3. The strain within the specimen decreases by 43.66% on average as eccentricity is increased from 1/12 to 1/3, whereas the strain value for eccentricity 0 is about 3 times lesser than that of eccentricity—1/12 as shown in Table 3.

The eccentric loading over CSRE prism specimens poses an uncertain situation, since the strain distribution over the section and randomness of fracture propagation within the prism is often complex.

The finite element modeling was capable of effectively predicting the stress-strain behaviour of CSRE prism specimens of different height-to-thickness ratios (3 and 4)

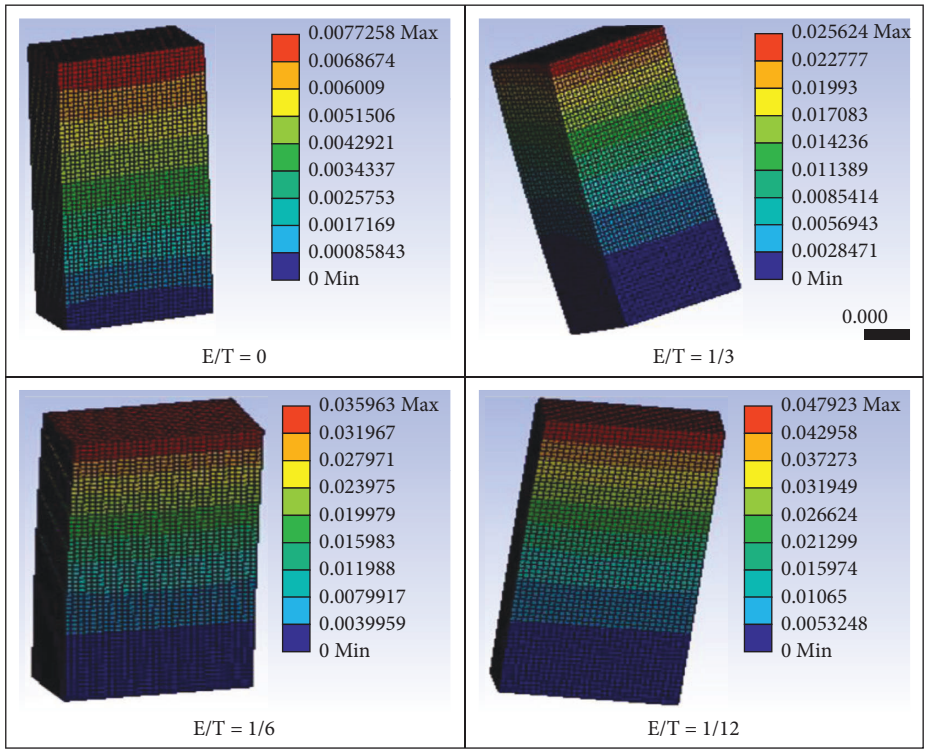

Figure 8: Deformation contours of specimens with H/T = 4.

along with their collapse/failure loads. The finite element model estimates of failure loads and the deformation values aid in the prediction of sufficiently accurate failure mechanisms.

4. Conclusions

The finite element analysis of cement-stabilized rammed Earth prisms of different height-to-thickness ratios (3 and 4) subjected to compressive load at different eccentricities 0, 1/3, 1/6, and 1/12 arrived at the following conclusions:

(1) The finite element model of CSRE prism having H/T ratio = 3 was subjected to varying magnitudes of concentric compressive load, and the deformation values obtained had a root mean square error of 1.95 mm in validation with the experimental results.

(2) Maximum compressive load—As the eccentricity of load application was increased from 0 to 1/6, the maximum compressive load decreased by 32% for the prism with H/T ratio = 3, whereas it decreases by 33.96% for the prism with H/T ratio = 4. When the eccentricity was increased from 1/6 to 1/3, the maximum compressive strength decreased by 42.8% in the prisms with H/T ratios = 3 and 4.

(3) Stress—The stress value was determined at the centre of the prism. For prisms with H/T ratios = 3 and 4, the stress value of the specimens remained almost the same for eccentricities 0 and 1/12. But, when the eccentricity of loading was increased from 1/6 to 1/3, the stress decreases by 31.09% for the prism with H/T ratio = 3, whereas it decreases by 25% for the prism with H/T ratio = 4.

(4) Strain—The strain value was determined at the centre of the prism. As the eccentricity was increased from 1/12 to 1/3, the strain decreases by 43.47% for the prism with H/T ratio = 3, whereas it decreases by 38.59% for the prism with H/T ratio = 4. But, the strain value for zero eccentricity was 3 times lesser than that of eccentricity of 1/12 for both the prisms with H/T ratios = 3 and 4.

The current research focuses solely on the behaviour of compressed cement-stabilized rammed Earth prism specimens. The limitation is that we are unable to generalize the results to a full-scale wall unit (commonly built rammed Earth construction). Future research should concentrate on performing a finite element analysis of any full-scale rammed Earth wall under compressive load and validate the results with experimental data.

Data Availability

The datasets generated during and/or analysed during this study are available from the authors on reasonable request.

Consent

Not Applicable.

Disclosure

ANSYS software was employed for FEM simulation.

Conflicts of Interest

The authors confirm that there are no conflicts of interest associated with this publication.

References

[1] D. Thompson, C. Osorio, and J. P. Osorio, "A review of current construction guidelines to inform the design of rammed earth houses in seismically active zones," *Journal of Building Engineering*, vol. 54, Article ID 104666, 2022.

[2] B. M. Ramesh, R. M. Vongole, Y. Naganna et al., "Valorization of incinerator bottom ash for the production of resource-efficient eco-friendly concrete: performance and toxicological characterization," *Architecture, Structures and Construction*, vol. 1, no. 1, pp. 65–78, 2021.

[3] G. Chang, C. M. Fiori, and C. Schexnayder, "Rammed earth: construction lessons from experience," *Practice Periodical on Structural Design and Construction*, vol. 18, no. 3, pp. 149–154, 2013.

[4] D. Easton and T. Easton, "Modern rammed earth construction techniques," in *Modern Earth Buildings, Woodhead Publishing Series in Energy*, M. R. Hall, R. Lindsay, and M. Krayenhoff, Eds., Woodhead Publishing, Cambridge, UK, pp. 364–384, 2012.

[5] H. Nouri and S. M. Hosseini, "Life cycle assessment of earthen materials for low-cost housing a comparison between rammed earth and fired clay bricks," *International Journal of Building Pathology and Adaptation*, 2021, ahead-of-print.

[6] R. A. Silva, D. V. Oliveira, T. Cristelo, N. Escobar, M. C. Soares, and E. Soares, "Rammed earth construction with granitic residual soils: the case study of northern Portugal," *Construction and Building Materials*, vol. 47, pp. 181–191, 2013.

[7] D. Tripura and K. Singh, "Structural behavior of rectangular cement-stabilized rammed earth column under compression," *Advances in Structural Engineering*, Springer India, New Delhi, India, pp. 2459–2469, 2015.

[8] P. A. Jaquin, *Analysis of Historic Rammed Earth Construction*, Durham University, UK, 2008, http://etheses.dur.ac.uk/2169/.

[9] Hb 195, *The Australian Earth Building Handbook*, Standards Australia International Ltd, Sydney, Australia, 2002.

[10] Nzs 4297, *Engineering Design of Earth Buildings"*, Standard, Newzeland, New zeland, 2020.

[11] Nzs 4298, *Materials and Construction for Earth Buildings*, Standard, Newzeland, New zeland, 2020.

[12] Nzs 4299, *Earth Buildings Not Requiring Specific Engineering Design*, Standard, Newzeland, New zeland, 2020.

[13] Astm E2392 05, *Standard Guide for Design of Earthen wall Building Systems*, Astm standard, PA, USA, 2005.

[14] S. Burroughs, "Soil property criteria for rammed earth stabilization," *Journal of Materials in Civil Engineering*, vol. 20, no. 3, pp. 264–273, 2008.

[15] V. Walker and P. Walker, "Structural capacity of rammed earth in compression," *Journal of Materials in Civil Engineering*, vol. 20, no. 3, pp. 230–238, 2008.

[16] M. E. Arslan, M. Yalama, and A. Yalama, "Structural behavior of rammed earth walls under lateral cyclic loading: a comparative experimental study," *Construction and Building Materials*, vol. 133, pp. 433–442, 2017.

[17] B. V. Venkatarama Reddy, V. Nanjunda Rao, and K. S. Nanjunda Rao, "Behaviour of cement stabilised rammed earth walls under concentric and eccentric gravity loading," *Earthen Dwellings and Structures: Current Status in Their Adoption*, Springer, Singapore, pp. 293–303, 2019.

[18] C. Ciancio and D. Ciancio, "Durability of cement-stabilised rammed earth: a case study in Western Australia," *Australian Journal of Civil Engineering*, vol. 14, no. 1, pp. 54–62, 2016.

[19] B. Khadka, "Rammed earth, as a sustainable and structurally safe green building: a housing solution in the era of global warming and climate change," *Asian Journal of Civil Engineering*, vol. 21, no. 1, pp. 119–136, 2020.

[20] M. Hallal, S. Sadek, and S. S. Najjar, "Evaluation of engineering characteristics of stabilized rammed-earth material sourced from natural fines-rich soil," *Journal of Materials in Civil Engineering*, vol. 30, no. 11, Article ID 04018273, 2018.

[21] S. M. S. Hussaini and V. Toufigh, "Strength and fracture behavior of rammed-earth materials," *Journal of Materials in Civil Engineering*, vol. 31, no. 10, Article ID 04019228, 2019.

[22] A. Suresh and K. B. Anand, "Strength and durability of rammed earth for walling," *Journal of Architectural Engineering*, vol. 23, no. 4, Article ID 06017004, 2017.

[23] T. T. Bui, A. Limam, and S. Maximilien, "Failure of rammed earth walls: from observations to quantifications," *Construction and Building Materials*, vol. 51, pp. 295–302, 2014.

[24] F. Ávila, E. Gallego, and R. Gallego, "Characterization of the mechanical and physical properties of unstabilized rammed earth: a review," *Construction and Building Materials*, vol. 270, Article ID 121435, 2021.

[25] H. Chazallon and C. Chazallon, "Finite element modelling of a rammed earth wall," *Construction and Building Materials*, vol. 25, no. 4, pp. 2112–2121, 2011.

[26] K. C. Shrestha, M. Aoki, and T. Aoki, "Assessment of out-of-plane behavior of rammed earth walls by pull-down tests," *International Journal of Architectural Heritage*, vol. 13, no. 2, pp. 273–287, 2019.

[27] V. Strazzeri, A. Elchalakani, and M. Elchalakani, "Micromechanics modelling of cement stabilised rammed earth," *Mechanics of Materials*, vol. 148, Article ID 103540, 2020.

[28] L. Miccoli, D. V. Oliveira, R. A. Silva, U. Schueremans, and L. Schueremans, "Static behaviour of rammed earth: experimental testing and finite element modelling," *Materials and Structures*, vol. 48, no. 10, pp. 3443–3456, 2015.

[29] Is 1905-1987, *Indian Standard Code of Practice for Structural Use of Unreinforced Masonry*, Indian Standard, Old Delhi, India, 2002.

[30] J. Narasimha Reddy, *Introduction to the Finite Element Method*, McGraw-Hill Education, New Delhi, 4th edition, 2019.

[31] O. C. Zienkiewicz, R. L. Taylor, and J. Zhu, *The Finite Element Method: Its Basis and Fundamentals*, Elsevier, Oxford, UK, 6th edition, 2005.

[32] Ansys Inc, *Ansys fluent user's guide, release 17.2*, 2016, https://www.ansys.com/.